Preu, J.; Jaeger, T.; Haramus, V.M.; Gutberlet, T.:

Use of small angle neutron scattering to study the interaction of angiotensin II with model membranes

In: European Biophysics Journal (2011) Springer

DOI: 10.1007/s00249-011-0675-6

European Biophysical Journal manuscript No.
(will be inserted by the editor)

Use of small angle neutron scattering to study the interaction of Angiotensin II with model membranes

Julia Preu · Timo Jaeger · Vasil Haramus · Thomas Gutberlet

Received: date / Accepted: date

Abstract The effect of the peptide hormone Angiotensin II (Ang II) on the structure of unilamellar and multilamellar dimyristoyl phosphatidylcholine (DMPC) vesicles is studied by small angle neutron scattering (SANS), dynamic light scattering (DLS) and differential scanning calorimetry (DSC). The calorimetry data indicates a weak interaction of Ang II with the surface of the membrane bilayer, as the pretransition persist during all experiments and the main transition gets only slightly shifted towards higher temperatures. From the SANS data we were able to confirm the calorimetric data and verify the interaction of the hormone with the membrane surface. At low temperatures, when the lipids are in the gel phase, more precisely in the ripple phase, the peptide penetrates in the headgroup region, but due to the close packing of the acyl chains, the hydrophobic region does not get affected. In a temperature region close to the region of the phase transition the hydrophibic core starts to get affected by the peptide, same is true for the fluid phase. Upon binding of the peptide the thickness of the head group increases and the scattering length density of the head group starts to rise, with increasing peptide concentrations. This interaction and binding to the membrane surface may be relevant for the relocation, binding and reconstitution of the Angiotensin receptors into the membrane. Second, the peptide adsorption to the membrane surface may contribute to the binding of Ang II in the active site of the receptor.

Keywords peptide-lipid interaction · small angle neutron scattering · Angiotensin II · DMPC · model membranes · hypertension

1 Introduction

Hypertension is a growing worldwide problem especially in the Western World. It is one of the major controllable risk factors associated with cardiovascular disease events such as myocardial infarcation, heart failure and end-stage diabetes (Pachori et al., 2001), (Dézsi, 2000), (Labinjoh et al., 2000), (Dimsdale et al., 1996), (Neutel et al., 1999), (MacMahon

F. Author
first address
Tel.: +123-45-678910
Fax: +123-45-678910
E-mail: fauthor@example.com

et al., 1990), (Organization, 2003).

In mammals the blood pressure is regulated by the renin-angiotensin system, which plays a critical role in circulatory homeostasis. Part of this system is the peptide hormone Angiotensin II (Asp-Arg-Val-Tyr-Ile-His-Pro-Phe), a potent vasoconstrictor that aids in the blood pressure regulation, as well as in body fluid balance maintenance. Ang II derives from the precursor angiotensinogen, through enzymatic reaction catalyzed by renin and the angiotensin converting enzyme (ACE). On the heart, acting in both endocrine and paracrine fashions Ang II regulates contractility, remodelling, growth, apoptosis, and reduces cell coupling and conduction velocity in cardiac muscles. The peptide acts on two major receptor subtypes, the Ang II type 1 receptor (AT_1-receptor) and the Ang II type 2 receptor (AT_2-receptor). Although both types of receptors were found in cardiac muscle cells, only the AT_1-receptor was found to mediate classical cardiovascular functions like blood pressure elevation, vasoconstriction, aldosterone release and renal absorption of water and sodium. From a patho-physiological point of view, like in renal diseases or hypertension, changes in the renin angiotensin system occurred (Hong et al., 2008).

The role of Ang II in causing chronic diseases is discussed in several publications (Ruiz-Ortega et al., 2003),(Striker et al., 2008), (Taylor, 1999), (de Gasparo et al., 2000). The ability of ACE inhibitors and AT_1-receptor antagonists to influence the cardiovascular status is consistent with an important role for the renin-angiotensin system in physiological and pathophysiological states (Costerousse et al., 1992), (Kurdi et al., 2005), (of health and human services, 2003). The inhibition of these enzyme (ACE) or AT_1 is believed to lower blood pressure. At present, the renin-angiotensin system has become a key target for drugs combating hypertension (Hong et al., 2008).

Hypertension can be treated by β-blockers, inhibiting the conversion of angiotensinogen to angiotensin I, or by specific inhibition of the AT_1-receptor by an Ang II antagonist like Losartan and its active derivate E-3174. Apart from action on the membrane bound receptor, an in vitro binding to lipids was described for Ang II, as well as Losartan. It was shown by ^{1}H-NMR that the binding of Ang II is depending on the pH of the surrounding medium and the temperature. Several amino acids of the peptide are involved in the binding to the lipids (Valensin et al., 1986). Later DSC and ^{31}P-NMR was used to further characterize the interaction of DPPC with Ang II (Mavromoustakos et al., 1996). The phase behaviour of the DPPC is affected by Ang II, as the main transition gets shifted towards higher temperatures and the pre-transition gets broadend. Results can be compared to similar studies on the interaction of Losartan with different lipids (Zoumpoulakis et al., 2003), (Theodoropoulou and Marsh, 1999), (Theodoropoulou and Marsh, 2000).

Applying SANS, DSC and DLS we studied the interaction of the peptide Ang II with a model membrane using pure DMPC vesicles. The main transition is occurring around 24 °C, making it possible to study the interaction in the gel, respectively ripple phase, and fluid phase of the lipid without facing the problem of peptide degradation, means the temperature dependent destruction of the peptide.

DSC is a versatile tool in life science allowing to study the thermotropic properties of a variety of materials and model systems (Bruylants et al., 2005). Especially for the study of membrane properties and changes calorimetric techniques are a vital tool (Westh, 2009). DSC was applied to study drug-lipid interactions as shown for vinorelbine (Koukoulitsa

et al., 2006), malatonin (Severcan et al., 2005) and the calcium-dependent antibiotic daptomycin (Jung et al., 2008). Work performed with peptide-lipid interaction focusses on synthetic peptides and peptides with antimicrobial properties, examples are aurein, citropin and maculatin (Seto et al., 2007), maganin (Ludtke et al., 1996), PGLa (Pabst et al., 2008) and other cell penetrating peptides (Alves et al., 2008).

SANS is a powerful technique to learn about the structure a variety of materials. Basically all biological macromolecules and the interaction among them can be studied by SANS. Single proteins and complexes (Petoukhov and Svergun, 2006), (Svergun and Koch, 2003) as well as polysaccharides, like cyclodextrins (V Burckbuchler and Amiel, 2008) are studied (Wang et al., 2009). A large variety of studies was dealing with lipids, their phases (Mason et al., 1999), (Winter, 2002) and the interaction with other classes of molecules. Bacterial membranes were used as sources (Mariani et al., 1997), but the majority of studies used synthetic lipids as model system (Kucerka et al., 2008), (Kučerka et al., 2007), (Nagle and Tristram-Nagle, 2000).

Due to the application of the contrast variation method (Knoll et al., 1981b) a variety of questions can be addressed using SANS. Bilayer thickness and interface area were studied (Balgavý et al., 2001; Pencer and Hallett, 2000), as well as the multilammelarity, structure and hydration of different lipid systems (Schmiedel et al., 2006; Tung et al., 2008). Of interest were the changes introduced upon mixing different lipids (Knoll et al., 1981a) as well as bilayer thickness responding to sterols (Pencer et al., 2005b), (Gallová et al., 2008), (Kucerka et al., 2009) and domains and rafts (Jacobson et al., 2007), (Pencer et al., 2005a).

The interaction of peptides and membranes was studied in combination with studies on cytotoxicity, like in the case of mellitin (Lundquist et al., 2008) and the development of new antimicrobial drugs (Huang, 2000), (Han et al., 2009).

So far no studies were deducted trying to study the interaction of peptides with membranes that don't lead to the formation of pores. Here we show, that it is possible to study the interaction of peptides with the membrane, even if the interaction does not lead to the formation of pores, but is based on a concentration-dependet adsorption process.

In addition to the SANS experiments DLS experiments were performed. The light scattering provided a first insight into changes in the hydrodynamic radius upon addition of the peptide in comparison to a pure DMPC sample. The resulting hydrodynamic radius was used for the data fitting of the SANS studies.

2 Methods

2.1 Materials

1,2-dimyristoyl-sn-glycero-3-phosphatidylcholine (DMPC) and the corresponding lipid with deuterated chains 1,2-dimyristoyl-(d54)-sn-glycero-phosphocholine (d54-DMPC) were purchased from Avanti Polar Lipids, Inc. (Alabaster, AL, USA). (4-(2-Hydroxyethyl) piperazine-1-ethanesulfonic acid sodium salt, (HEPES 99.5 % pure), Angiotensin II (human actetat,

93 % pure), NaCl (analytical grade) and D_2O (99.9 % deuteration) from Sigma Aldrich. All chemicals were used without further purification.

2.2 Differential Scanning Calorimetry

DSC experiments were performed on a high sensitivity differential scanning calorimeter (Microcal VP-DSC, Northampton, MA, USA), with a cell volume of 0.51 ml. The reference cell contained pure water and the heating rate was 5 ° C/h. At least two calorimetric scans were performed with each sample to test reproducibility. Data evaluation was performed using a macro running with Igor Pro (WaveMetrics, Inc., Portland, OR 97223, USA). The raw data was normalized by the lipid concentration and the base line was substracted. The phase transition temperatures were taken at peak values of the heat capacity, c_p, and the calorimetric enthalpy ΔH was calculated by integrating the peak areas. In addition the position and area under the pre-transition peak was determined.

2.3 Dynamic Light Scattering

For the light scattering experiments an ALV-5000 Multiple Tau Digital Correlator together with a HeNe-Laser at a wavelength of 632.8 nm was used. The temperature was controlled with an external heating circulator (F25-ME, Julabo, Seelbach, Germany). For aqueous solutions a refractive index of 1.3320 and a viscosity of 0.890001 cp is assumed (1 cp = 1 centipoise = 0.001 g cm^{-1} s^{-1}). The hydrodynamic radius was calculated

$$R_h = \frac{kT}{6\pi\eta\Gamma} q^2 \tag{1}$$

with

$$q = \frac{4\pi n sin(\frac{\theta}{2})}{\lambda} \tag{2}$$

n- refractive index, λ-wavelength, θ-scattering angle, k-Boltzmann's constant, η-solvent viscosity, Γ-average decay rate.

2.4 Small Angle Neutron Scattering

For the SANS experiments a HEPES buffer (10 mM HEPES, 100 mM NaCl) in D_2O was used, applying the concept of contrast variation (Knoll et al., 1981b). Using heavy water the pD was adjusted to a value equivalent to pH 7.6 using the conversion pD = 0.929 pH meter reading + 0.42 (Lowe and Smith, 1973). Ang II was added to the buffer to final concentrations of 0.1 mM, 0.5 mM and 1 mM. As a control a pure lipid sample was used.

Small-angle neutron scattering experiments were performed at the SANS 1 instrument at the FRG 1 research reactor at the GKSS research center, located in Geesthacht, Germany (Stuhrmann et al., 1995). The neutron wavelength was 4.5 Å, and the wavelength resolution was 10 % (full width at half-maximum value). The range of scattering vectors

($0.004 < q < 0.25$ Å^{-1}) was obtained using two sample-to-detector distances (2 and 8 m). For the SANS measurements, the samples were equilibrated at various temperatures with a precision of $\pm$ 0.5 °C in quartz cuvettes (Hellma, Muellheim, Germany) with a path length of 1 mm. The raw SANS spectra were corrected for backgrounds from the solvent, sample cell, and other sources by conventional procedures. The two-dimensional isotropic scattering spectra were averaged, converted to an absolute scale, and corrected for detector efficiency by substracting by the incoherent scattering spectrum of pure D_2O which was measured within the same cells as the samples.

2.4.1 Vesicle preparation

For the DLS and SANS experiments unilamellar vesicles were used. DMPC, d54-DMPC, respectively, was immersed in the different buffers to a final concentration of 5 mM for DLS and 10 mM for SANS, producing multilamellar vesicles (MLVs). The temperature of the dispersion was kept above 40 °C and, after vortexing, unilamellar extruded vesicles were produced using an Avanti Mini Extruder (Avanti Polar Lipids, Alabaster, AL) and an Isopore ^{TM} polycarbonate filter (Millipore, Billerica, MA, USA) of 0.1 μm pore size. As extruded ULVs are generally contaminated with pauci lamellar vesicles (PLVs) a small vesicle size was used to maximize the amount of ULVs (Kucerka et al., 2007). The MLVs were extruded an odd number of passes to avoid contamination of the sample by large and multilamellar vesicles, which might not have passed through the filter.

2.4.2 SANS data analysis

The analysis of the SANS data was performed using the software package described by Kline (Kline, 2006) based on macros running under Igor Pro (WaveMetrics, Inc., Portland, OR 97223, USA). This data analysis software provides the possibilty to undergo non-linear data fitting, based on a variety of included form factors. To analyse our data in particular the combination of form factors became necessary. Following the separated form factor approach, as published by Kiselev et al. (Kiselev et al., 2002), two form factors were summed up in order to reflect the changes in the sample with an appropriate model. One of the two form factors describes a lamellae, taking into account different scattering length densities for the chain and the head group region (Nallet et al., 1993), (Javierre et al., 2000). Second a form factor representing a polydisperse vesicle (Bartlett and Ottewill, 1992) was used. The initially used scattering length densities (SLDs) were calculated values. The scattering length values for D_2O were fixed. For the bilayer thickness, the length of the head group and the hydrophobic region of pure DMPC literature values were used as an orientation (Nagle and Tristram-Nagle, 2000), (Kucerka et al., 2008), (Kiselev et al., 2006).

Form factor of polydisperse vesicle

The form factor (FF) for a vesicle with a polydisperse core with constant shell thickness was used as described by Bartlett and Ottewill (Bartlett and Ottewill, 1992). To derive the relation and to define the parameters of the FF a suspension of noninteracting particles is considered showing only coherent scattering and no multiple scattering.

$$\frac{d\Sigma}{d\omega}(\mathbf{q}) = n\left\langle \left| \sum_{i(v)} b_i exp(i\mathbf{q}\cdot\mathbf{r}_i)\right|^2 \right\rangle \tag{3}$$

b_i the atomic scattering length density, n is the number density of particles and the sum is adding over all atoms in the particle volume v. As SANS experiments do not yield information on the atomic scale the atomic scattering lengths b_i can be replaced by the locally averaged scattering length density defined as

$$\rho(\mathbf{r}) = \sum_i b_i \delta(\mathbf{r} - \mathbf{r}_i) \tag{4}$$

b_i is the scattering length of the atom at the position r_i. Replacing the sum in Eq. 3 by an integral yields an expression for the scattering from a suspension of noninteracting spheres

$$\frac{d\Sigma}{d\omega}(\mathbf{q}) = nF(\mathbf{q})^2 \tag{5}$$

where the scattering amplitude id defined by the Fourier transform

$$F(\mathbf{q}) = \int [\rho(\mathbf{r}) - \rho_m] exp(i\mathbf{q}\cdot\mathbf{r}) d\mathbf{r} \tag{6}$$

ρ_m is the scattering length density of the buffer. Assuming a spherically symmetric profile $\rho(r)$ the scattering amplitude for a single particle reduces to

$$F(q) = 4\pi \int r^2 [\rho(r) - \rho_m] \frac{sin\ qr}{qr} dr \tag{7}$$

The scattering profile has the form

$$\rho(r) = \begin{cases} \rho_c & r \le r_c \\ \rho_s & r_c < r \le r_c + \Delta \end{cases} \tag{8}$$

with r_c the radius of the spherical core and the scattering length density ρ_c surrounded by a shell of the thickness Δ with the scattering length density ρ_s. Correspondingly the particle scattering amplitude can be written as

$$F(x) = \frac{4\pi}{q^3}(\rho_s - \rho_c)\{\gamma j(x + \delta x) - j(x)\} \tag{9}$$

$\rho = \Delta / r_c$ and $x = qr_c$. The function $j(x) = sin\ x\ -\ x\ cos\ x$. The scaled medium contrast $\gamma = (\rho_m - \rho_s)/(\rho_c - \rho_s)$ determines the relative proportion of the scattering from the core or the shell. To take into account the polydispersity of the vesicle a particle distribution is introduced. For this Eq. 5 needs to be averaged over the particle size distribution, assuming that only the size of the particle core is varying whereas the shell thickness Δ is constant. For this the single particle FF $F^2(qr_c)$ is replaced by the size average

$$\bar{F}^2(q\bar{r}_c) = \int_0^\infty G(r_c) F^2(qr_c) dr_c \tag{10}$$

$G(r_c)$ is the normalized probability to find a particle with a core radius between r_c and $r_c + dr_c$, $\bar{r}_c$ is the mean core radius. For the distribution of the mean core radius a Schulz distribution is picked. The normalized form of this distribution is

$$G(r_c) = \frac{r_c^Z}{\Gamma(Z+1)} \left(\frac{Z+1}{\bar{r}_c}\right)^{Z+1} \cdot exp\left[-\frac{r_c}{\bar{r}_c}(Z+1)\right] \tag{11}$$

with $\bar{r}_c$ is the mean core radius and Z is related to the normalized polydispersity σ_c of the particle core radius distribution

$$\sigma_c^2 = \left(\frac{\bar{r_c^2}}{\bar{r_c^2}} - 1 \right) = \frac{1}{Z+1} \tag{12}$$

.

Lamellar form factor

For the description of the bilayer a lamellar FF was used as published by (Nallet et al., 1993) (Javierre et al., 2000). To describe the different segments of the bilayer a two-square profile is defined, with two variable parameters for each segment. The segments are the headgroup with the thickness δ_H and the scattering length density σ_H and accordingly the tail with the thickness δ_T and the scattering length density σ_T. To derive the form factor the following assumptions were made

$$\Delta\sigma_H = \sigma_H - \sigma_{solvent} \tag{13}$$

$$\Delta\sigma_T = \sigma_T - \sigma_H \tag{14}$$

$$2(\delta_H + \delta_T) = \text{ total bilayer thickness} \tag{15}$$

The resulting FF has the following format.

$$P(q) = \frac{4}{q^2} \left\{ \Delta\rho_H \left[sin\left[q(\rho_H + \rho_T) \right] - sin(q\rho_T) \right] + \Delta\rho_T sin(q\delta_T) \right\}^2 \tag{16}$$

3 Results

3.1 Differential Scanning Calorimetry

In the DSC measurements we investigated pure DMPC samples and the same concentration of DMPC with different concentrations of Ang II. The data was normalized by the lipid concentration and the baseline was subtracted. In Table 1 the thermodynamic data resulting from the DSC scans are listed and in Figure 1 the corresponding thermotropic traces are shown. The tables comprises the values for the peak temperatures of the pre and main transition. In addition the enthalpy was calculated by integration of the area under the main transition peak and the pre-transition peak. Another indicator for changes in the phase behavior is the upper phase boundary, representing the temperature where half of the lipids are in the gel state and the other half is in the fluid state (Feigenson, 2007).

The results for pure DMPC dispersions are in good agreement with previous studies (Heimburg, 2000). For pure DMPC a sharp main transition peak just below 24 °C and in addition a pre-transition around 14 °C is expected. From our measurement a temperature of 23.6 °C for the main transition and 13.8 °C for the pre-transition resulted. Accordingly the enthalpy for the main transition was calculated as 6.55 kJ/mol and as 1.37 kJ/mol for the pre-transition.

With increasing concentrations of Ang II the peak temperature gets shifted towards higher

temperatures and the enthalpy increases. For the main transition the enthalpy increases constantly with increasing concentrations of the peptide. The initial addition of the peptide leads to an increase in enthalpy by about 1.5 kJ/mol. For the higher concentrations a smaller increase in the enthalpy of the main transition can be observed. For ever higher ratio the enthalpy is increasing by about 600 J/mol.

For the pre-transition the enthalpy changes also with the addition of the peptide. At the highest lipid:peptide ratio (1:100) an increase of 72 J/mol was calculated. For the lipid peptide ratio of 1:50 the enthalpy raises more than 200 J/mol. Finally for the peptide:lipid ratio of 1:10 the enthalpy increases again by about 200 J/mol compared to the previous ratio. For the highest concentration of the peptide and a ratio of peptide to lipid of 1:5 the enthalpy of the pre-transition drops slightly compared to the next lower peptide concentration.

Studying the temperature change induced by the peptide, again the temperature of the main transition and for the pre-transition can be compared for pure DMPC and samples containing Ang II in addition. The temperature of the main transition is shifted between 0.4 °C and 0.6 °C as a response to Ang II binding. Comparing the temperature of the pure DMPC sample and after addition of peptide with a peptide:lipid ratio of 1:100 an increase in the transition temperature of 0.4 °C is observed. For the higher peptide concentrations only a small further increase of the temperature can be seen. A similar result gives the analysis of the pre-transition temperature. The temperature raises by 1.3 °C for the addition of the peptide at the lowest concentration and by around 0.2 °C for the next higher peptide concentration. For the higher peptide concentrations the result is different. The temperature always stays above 15 °C. Another indicator for changes occurring at the membrane is the upper phase boundary, the temperature were an equal number of lipids are in the fluid state and in the gel state. For DMPC the upper phase boundary was calculated as 23.64 °C and it raises by 0.42 °C for the two lowest peptide concentrations. For the two higher concentrations the temperature raises by 0.46 °C.

As the pretransition temperature is more sensitive to changes at the membrane surface a change in the pre-transition temperature points towards an interaction of the peptide with the membrane surface. Upon molecules interacting not only with the surface, but at the interface region or in the hydrophobic region the pre-transiton will vanish completely. For the present study the pretransition remains visible in the data and gets shifted towards higher temperatures by more than 1 °C. The peak broadens and the enthalpy increases.

The enthalpy of the main transition is also increasing except for the highest peptide concentration. This non-linear increase in the enthalpy supports a weak binding and interaction with the surface of the bilayer. With decreasing lipid:peptide ratio a saturation level is reached, where no further peptide molecules bind to the surface. We will further elaborate on this fact after introducing the results from the scattering experiments. The results from the DSC gave a first insight into the interaction of the membrane with the peptide and it can be concluded that the interaction is weak and mainly taking place at the surface of the membrane.

3.2 Dynamic Light Scattering

The dynamic light scattering was used as to get a first insight into the structural changes occurring in the vesicles upon addition of the peptide, results are shown in Figure 2 and Tabelle 2. The main information gained from light scattering experiments is the hydrodynamic radius. For the experiments extruded vesicles were used and the buffer contained the peptide in different concentrations. As a main result we could show that the hydrodynamic radius increased upon addition of the peptide. Initially a hydrodynamic radius about 60 nm was measured for DMPC above the phase transition. Lowering the temperature leads to a gradual increase in the hydrodynamic radius. Below the phase transition the radius reaches around 90 nm. The difference in radius can be explained due to the decreased mobility of the particles at low temperatures.

3.3 Small Angle Neutron Scattering

To get an insight into the structural changes occurring on the membrane level small angle neutron scattering was applied. To make sure that only single particle form factors are measured a diluted dispersion was used, containing about 1 w% samples. The dispersion was extruded to avoid aggregation and periodic packing of bilayers that may give rise to Bragg peaks. All samples were measured with respect to the different lipid phases at 15 °C, 22 °C and 35 °C with respect to the different lipid phases.

After general corrections, averaging and integration of the data a detailed data analysis was performed using the separated form factor (SFF) approach (Kiselev et al., 2002). Two form factors (FFs) were combined, leading to the possibility to describe the vesicle and the structure of the lamellae at the same time. In detail the first FF describes the tail length and the thickness of the head group and the corresponding scattering length densities (SLDs), respectively. The second FF is used to describe the overall structure of the vesicle, taking into account the vesicle size, the bilayer thickness and the polydispersity of the vesicle. For all experiments chain deuterated DMPC (d54-DMPC) was used, having the advantage that a large SLD contrast difference exists between the head group and the acyl chains. A penetration of the peptide into the hydrophobic core would become visible instantly in the data. The results are displayed in Figure 3 and in the Tables 3 for the different temperatures.

At first the data from the pure d54-DMPC samples were fitted, starting with the data set where the lipids are in the fluid state as only limited literature is available for the gel, respectively ripple phase. For d54-DMPC in the fluid phase literature values were taken were possible or the values for DPPC were used taking into account the difference in tail length (Nagle and Tristram-Nagle, 2000), (Kucerka et al., 2008), (Kiselev et al., 2006). Based on this initial data, a fit to the experimental data became possible. For d54-DMPC in the fluid phase the tail length was fitted to 13.75 Å $\pm$ 0.06 Å with a SLD of $7.2 \cdot 10^{-6}$ Å $^{-2}$ and for the head group a thickness of 5.24 $\pm$ 0.17 Å with a SLD of $1.2 \cdot 10^{-6}$ Å $^{-2} \pm 0.1 \cdot 10^{-6}$ Å $^{-2}$. This sums up a membrane thickness of 37.98 Å which is in good agreement with literature values (Kucerka et al., 2008), (Kiselev et al., 2006). With these parameters the according fits for the d54-DMPC data sets at lower temperatures were performed. For the sample at 15 °C a smaller thickness of the head group and a longer hydrophobic region is expected. The head group is slightly tilted in the ripple phase and therefore the head group appears smaller in the ripple phase. Unmolten acyl chains are about 20 % longer than the molten ones, making a difference of about 3 Å between the two states. For the sample at 22 °C the values should lie in between. The resulting thickness of the head group at 15 °C is 4 Å and 4.99 Å at 22 °C,

correspondingly the tail length at 15 °C was fitted with 16.3 Å and for 22 °C with 15 Å . Based on the fits for the pure lipid samples the data with increasing peptide:lipid ratios were fitted. At 15 °C the acyl chains were fitted with a constant length of 16.3 Å ± 0.32 Å . The thickness of the head group increased with the amount of peptide added, from 4 Å ± 0.06 Å for pure d54-DMPC to 4.2 Å ± 0.06 Å at a peptide:lipid ratio of 1:100, 5 Å ± 0.06 Å at a peptide:lipide ratio of 1:50 and finally to 7.5 Å ± 0.08 Å at a ratio of 1:10. The fits for the sample incubated at 22 °C resulted in an slight decrease of the tail length, going from 14.5 Å ± 0.28 Å , 14.2 Å ± 0.28 Å to 13.6 Å ± 0.26 Å with increasing peptide concentration. In turn the head group size increases from 4.99 Å ± 0.19 Å over 6.09 Å ± 0.17 Å and 7.75 Å ± 0.14 Å to 7.89 Å ± 0.11 Å for the highest peptide amount in the sample. In the fluid phase, at 35 °C, the tail length again decreases slightly from 13.52 Å ± 0.25 Å (peptide:lipid ratio 1:100) to 13.4 Å ± 0.26 Å (1:50) down to 13 Å ± 0.26 Å (1:10). The fitted values for the head group are 5.73 Å ± 0.18 Å , 6.65 Å ± 0.19 Å and 7.58 Å ± 0.15 Å with increasing peptide:lipid ratio.

In addition to changes in the length of the head group and the hydrophobic tail, the SLDs were adjusted during the fitting procedure. At 15 °C the SLD for the head group changes from $1.1 \cdot 10^{-6}$ Å $^{-2} \pm 0.01 \cdot 10^{-6}$ Å $^{-2}$ over $1.9 \cdot 10^{-6}$ Å $^{-2} \pm 0.01 \cdot 10^{-6}$ Å $^{-2}$ to $3.3 \cdot 10^{-6}$ Å $^{-2} \pm 0.03 \cdot 10^{-6}$Å $^{-2}$ and accordingly for the acyl chains drops slightly to $7.1 \cdot 10^{-6}$ Å $^{-2}$. At 22 °C the SLD of the head group also increases with increasing amounts of peptides by around $1 \cdot 10^{-6}$ Å $^{-2}$, whereas the SLD of the tails stays constant. Finally for 35 °C the SLD of the head group stays constant for the low peptide concentrations, but increases to $2.98 \cdot 10^{-6}$ Å $^{-2}$ for a peptide:lipid ratio of 1:10. The SLD of the tail is only insignificantly decreasing.

4 Discussion

From the results of the DSC and the SANS data a concentration-dependent model for the binding of Ang II to membranes can be suggested. The DSC experiments resulted in a shift of the main transition towards higher temperatures, hence a preferential binding to the gel phase is indicated. This is supported by the SANS data, as the increase in head group thickness at 15 °C is the highest one for all the studied temperatures, accompanied by the highest increase in the SLD of the head group. The thickness of the tail stays unaffected, which can be explained by the close packing of the acyl chains in the gel phase, that can not be accessed by the peptide, even not at high peptide concentrations.

At 35 °C the head group thickness also increases upon the binding of the peptide and in addition the tail length is slightly decreased, pointing towards a penetration of the peptide into the interface of the head group and the acyl chains. Close to the phase transition at 22 °C this effect is even more pronounced, as the membrane is most flexible in this temperature region. This tendency is supported by the corresponding changes in the SLDs. At all temperatures the SLD of the tails stays basically constant, where as it increases for the head group region. This increase in the SLD is caused by the interaction of the peptide. The SLD of the peptide is lower than the one of the lipid headgroup, but the penetration of D_2O molecules into this region causes an increase in the SLD. For the samples at 22 °C the SLD of the tails, again stays constant and the one for the head group is increased. At 35 °C the SLD of the tails again can be considered as constant and the SLD of the head only changes

for high concentrations of peptides.

Our data gives clear evidence for the adsorption of the peptide to the membrane surface, a tendency for preferred binding to the fluid phase is evident and only at high concentrations the peptide starts to penetrate closer to the interface between the head group and the acyl chains.

Looking at the previously published studies it becomes evident that they focus on the structure of the peptide in different chemical environments. Various experiments aimed to elucidate the peptide structure in the receptor, which would lead to a basis for rational design of Ang II peptidomimetics with potent antagonist properties. So far no experimental structural information of the peptide bound to the AT_1 receptor is available and therefore a number of secondary-structural features under various conditions with the attempt to mimic the natural environment of the receptor were performed (Surewicz and Mantsch, 1988; Garcia et al., 1992; Shin and Yoo, 1996; Cho and Asher, 1996; Joseph et al., 1995) as well as in vitro binding studies of Losartan or Ang II (Chansel et al., 1994).

Fatigati and Peach postulated a lipid milieu as local environment for Ang II therefore our interest focuses on the concentration-dependent interaction of Ang II on model membranes and the structural changes induced by the insertion, studied at different temperatures (Fatigati and Peach, 1988).

For the AT_1 receptor antagonist Losartan a membrane-mediated binding to the receptor was suggested, assuming the binding to the membrane surface, diffusing through the membrane bilayer, before binding to the receptor (Zoumpoulakis et al., 2003). A similar mechanism may be plausible for Ang II, where the presence of the peptide is necessary for the translocation of the receptor into the membrane. Ang II may alter the membrane properties that the insertion of the receptor gets facilitated and the binding of Ang II to the active pocket in the receptor is further supported by prior binding to the membrane surface. Along with this discussion our study provides new insight into the interaction of Ang II with model membranes in this case DMPC vesicles. It can be concluded that Ang II influences the hydration of the head group and that this facilitates the insertion of the receptor in the membrane and subsequently the activation of the receptor by peptide.

5 Conclusion

In conclusion we could show that Ang II is in interaction with the surface of the membrane depending on the peptide concentration and the phase of the lipids. At low temperatures the peptide stays on the surface and in the head group region. With increasing temperatures and increased fluctuations close to the temperature of the phase transition a deeper penetration of the peptide into the bilayer is enabled. Ang II is altering the hydration of the lipid head groups, facilitating possible refolding of the receptor in the membrane and the subsequent binding of Ang II in the active site.

In addition here we showed, that SANS is a suitable tool to study the interaction of a membrane-active peptide with the lipid surface. Key is the data analysis, as the combination of separated form factors gives rise to a variety of parameters that can describe a system on the level of the lamellae up to changes in the overall vesicle size. SANS and the method

of contrast variation gives rise to an increase in contrast enabling a label-free sample preparation. The use of chain deuterated DMPC has the advantage that the contrast between the head group and the acyl chains is comparably high as the one between D_2O and the head group.

Table 1 Enthalpy and peak temperature of the main transition and pre transition, as well as the upper phase boundary for pure DMPC dispersions and DMPC mixed with Ang II in the peptide: lipid ratios 1:100, 1:50, 1:10, 1:5

sample	DMPC	1:100	1:50	1:10	1:5
Enthalpy main transition $C_p(J/mol \cdot deg)$	6558.6 ± 918.2	8040.47 ± 1225.66	8818.38 ± 1234.57	9602.9 ± 1344.4	10361.4 ± 1450.59
pre transition $C_p(J/mol \cdot deg)$	1374.09 ± 192.37	1446.95 ± 202.573	1645 ± 230.3	1856.25 ± 259.87	1765.54 ± 247.17
peak temperature main temperature (°C)	23.599	23.99	24.0091	24.0416	24.0349
peak temperature pre temperature (°C)	13.8415	15.19	15.3781	15.1215	15.053
Upper phase boundary (°C)	23.6455	24.0719	24.075	24.1118	24.166

Table 2 Hydrodynamic radii from dynamic light scattering experiments for pure DMPC dispersions and lipid peptide mixtures with different ratio, shown for temperatures between 35 and 5 ° C

temperature	hydrodynamic radius (nm)				
(°C)	(1:100)	(1:50)	(1:10)	(1:5)	DMPC
35	59.01 ± 4.53	56.74 ± 4.58	57.31 ± 4.22	52.77 ± 4.25	53.15 ± 4.72
33	58.72 ± 4.51	56.46 ± 4.69	58.70 ± 4.28	53.58 ± 4.19	52.49 ± 4.69
31	60.43 ± 4.64	58.11 ± 4.84	60.57 ± 4.37	54.66± 4.35	54.45 ± 4.83
29	62.16 ± 4.78	59.77 ± 4.96	62.12 ± 4.49	56.23± 4.52	56.51 ± 4.97
27	64.38 ± 4.95	61.90 ± 5	62.59 ± 4.55	56.99 ± 4.6	57.61 ± 5.15
26	65.40 ± 5.03	62.88 ± 5.14	64.31 ± 4.72	59 ± 4.72	59 ± 5.23
25	67.84 ± 5.21	65.23 ± 5.37	67.15 ± 4.76	59.60 ± 4.81	60.17 ± 5.42
24	69.01 ± 5.3	66.36 ± 5.51	68.95 ± 4.9	61.26 ± 4.97	62.16 ± 5.52
23	71.25 ± 5.48	68.51 ± 5.51	68.89 ± 5	62.58 ± 5.06	63.26 ± 5.7
22	72.96 ± 5.61	70.16 ± 5.78	72.37 ± 5.11	63.99 ± 5.15	64.41 ± 5.83
21	73.84 ± 5.68	71.00 ± 5.81	72.65 ± 5.24	65.58 ± 5.2	65.05 ± 5.9
20	76.35 ± 5.87	73.42 ± 6.05	75.71 ± 5.32	66.51 ± 5.53	69.14 ± 6.1
19	79.48 ± 6.11	76.42 ± 6.09	76.17 ± 5.27	65.97 ± 5.4	67.54 ± 6.35
18	80.07 ± 6.15	76.99 ± 6.28	78.61 ± 5.46	68.28 ± 5.6	70.09 ± 6.4
16	82.35 ± 6.33	79.18 ± 6.45	80.70 ± 5.51	68.87 ± 5.59	69.99 ± 6.58
14	85.29 ± 6.56	82.01 ± 6.49	81.18 ± 5.8	72.54 ± 5.92	74.04 ± 6.82
12	88.19 ± 6.78	84.8 ± 6.63	82.89 ± 5.85	73.12 ± 6.05	75.68 ± 7.05
10	88.48 ± 6.8	85.08 ± 6.93	86.71 ± 6.04	75.52 ± 6.14	76.78 ± 7.07
8	93.28 ± 7.17	89.70 ± 6.97	87.23 ± 6.13	76.71 ± 6.35	79.43 ± 7.46
6	93.38 ± 7.18	89.79 ± 7.3	91.36 ± 6.36	79.58 ± 6.5	81.33 ± 7.47
5		92.67 ± 7.41	82.11 ± 6.56	84.13 ± 6.73	

Table 3 Small angle neutron scattering data fitting parameter

temp (°C)	sample	d54-DMPC	1:100	1:50	1:10
15	tail length (Å)	16.3 ± 0.32	16.3 ± 0.32	16.3 ± 0.32	16.3 ± 0.32
	headgroup thickness (Å)	4 ± 0.06	4.2 ± 0.06	5.0 ± 0.06	7.5 ± 0.08
	SLD tails ($Å^{-2}$)	$7.25 \cdot 10^{-6}$	$7.2 \cdot 10^{-6}$	$7.15 \cdot 10^{-6}$	$7.1 \cdot 10^{-6}$
	SLD headgroup ($Å^{-2}$)	$1.1 \cdot 10^{-6} \pm 0.01 \cdot 10^{-6}$	$1.1 \cdot 10^{-6} \pm 0.01 \cdot 10^{-6}$	$1.9 \cdot 10^{-6} \pm 0.01 \cdot 10^{-6}$	$3.3 \cdot 10^{-6} \pm 0.03 \cdot 10^{-6}$
	SLD solvent ($Å^{-2}$)	$6.36 \cdot 10^{-6}$	$6.36 \cdot 10^{-6}$	$6.36 \cdot 10^{-6}$	$6.36 \cdot 10^{-6}$
	background (cm^{-1})	0.009	0.003	0.002	0.001
	average core radius (Å)	740	780	820	880
	average shell thickness (Å)	40.8	40.6	43	41
	overall polydispersity	1 ± 0.03	0.90 ± 0.01	0.96 ± 0.02	1 ± 0.02
	SLD core and solvent ($Å^{-2}$)	$6.36 \cdot 10^{-6}$	$6.36 \cdot 10^{-6}$	$6.36 \cdot 10^{-6}$	$6.36 \cdot 10^{-6}$
	SLD shell ($Å^{-2}$)	$4.78 \cdot 10^{-6}$	$4.78 \cdot 10^{-6}$	$4.78 \cdot 10^{-6}$	$4.78 \cdot 10^{-6}$
22	tail length (Å)	15 ± 0.3	14.5 ± 0.28	14.2 ± 0.28	13.6 ± 0.26
	headgroup thickness (Å)	4.99 ± 0.19	6.09 ± 0.17	7.75 ± 0.14	7.89 ± 0.11
	SLD tails ($Å^{-2}$)	$7.2 \cdot 10^{-6}$	$7.2 \cdot 10^{-6}$	$7.15 \cdot 10^{-6}$	$7.15 \cdot 10^{-6}$
	SLD headgroup ($Å^{-2}$)	$1.45 \cdot 10^{-6} \pm 0.12 \cdot 10^{-6}$	$1.6 \cdot 10^{-6} \pm 0.1 \cdot 10^{-6}$	$2.35 \cdot 10^{-6} \pm 0.007 \cdot 10^{-6}$	$2.6 \cdot 10^{-6} \pm 0.1 \cdot 10^{-6}$
	SLD solvent ($Å^{-2}$)	$6.36 \cdot 10^{-6}$	$6.36 \cdot 10^{-6}$	$6.36 \cdot 10^{-6}$	$6.36 \cdot 10^{-6}$
	background (cm^{-1})	0.009	0.003	0.002	0.004
	average core radius (Å)	750	740	750	740
	average shell thickness (Å)	41	43	45	42
	overall polydispersity	0.78 ± 0.01	0.76 ± 0.01	0.83 ± 0.02	1 ± 0.02
	SLD core and solvent ($Å^{-2}$)	$6.36 \cdot 10^{-6}$	$6.36 \cdot 10^{-6}$	$6.36 \cdot 10^{-6}$	$6.36 \cdot 10^{-6}$
	SLD shell ($Å^{-2}$)	$4.78 \cdot 10^{-6}$	$4.78 \cdot 10^{-6}$	$4.78 \cdot 10^{-6}$	$4.78 \cdot 10^{-6}$
35	tail length (Å)	13.75 ± 0.06	13.52 ± 0.25	13.4 ± 0.26	13.0 ± 0.26
	headgroup thickness (Å)	5.24 ± 0.17	5.73 ± 0.18	6.65 ± 0.19	7.58 ± 0.15
	SLD tails ($Å^{-2}$)	$7.2 \cdot 10^{-6}$	$7.2 \cdot 10^{-6}$	$7.1 \cdot 10^{-6}$	$7.0 \cdot 10^{-6}$
	SLD headgroup ($Å^{-2}$)	$1.2 \cdot 10^{-6} \pm 0.1 \cdot 10^{-6}$	$1.2 \cdot 10^{-6} \pm 0.1 \cdot 10^{-6}$	$1.5 \cdot 10^{-6} \pm 0.1 \cdot 10^{-6}$	$2.98 \cdot 10^{-6} \pm 0.006 \cdot 10^{-6}$
	SLD solvent ($Å^{-2}$)	$6.36 \cdot 10^{-6}$	$6.36 \cdot 10^{-6}$	$6.36 \cdot 10^{-6}$	$6.36 \cdot 10^{-6}$
	background (cm^{-1})	0.009	0.003	0.007	0.004
	average core radius (Å)	510	520	540	560
	average shell thickness (Å)	38	39	41	41
	overall polydispersity	0.93 ± 0.02	0.84 ± 0.02	0.86 ± 0.01	0.88 ± 0.02
	SLD core and solvent ($Å^{-2}$)	$6.36 \cdot 10^{-6}$	$6.36 \cdot 10^{-6}$	$6.36 \cdot 10^{-6}$	$6.36 \cdot 10^{-6}$
	SLD shell ($Å^{-2}$)	$4.78 \cdot 10^{-6}$	$4.78 \cdot 10^{-6}$	$4.78 \cdot 10^{-6}$	$4.78 \cdot 10^{-6}$

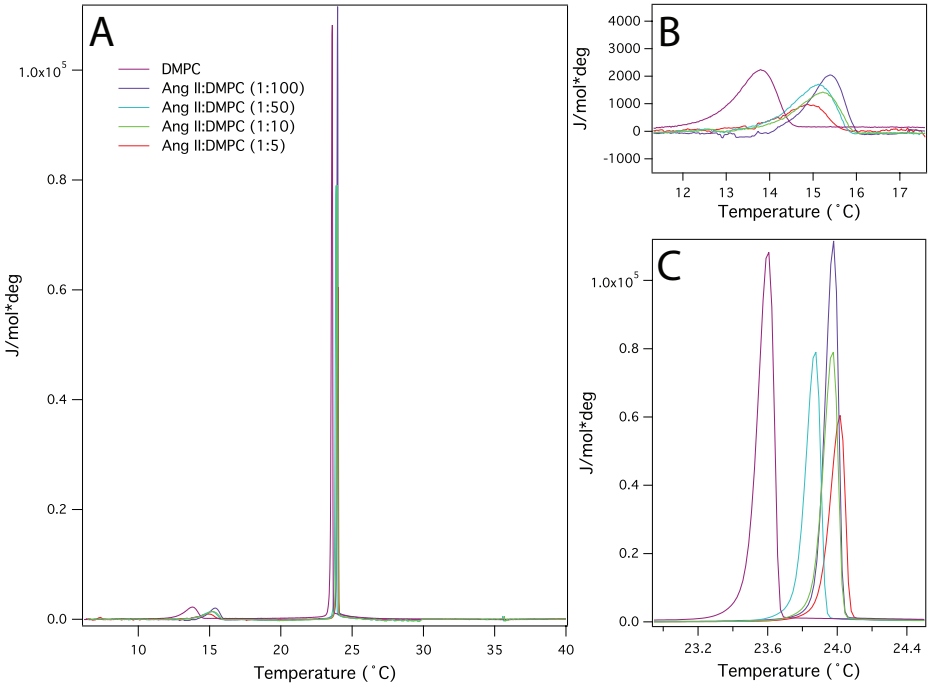

Fig. 1 Excess heat capacity curves of DMPC and mixtures of peptide and lipid with ratios of 1:100, 1:50, 1:10, 1:5), Panel A displays the whole thermogram. Panel B shows a magnification of the pretransition region and Panel C a magnification of the main transition peaks

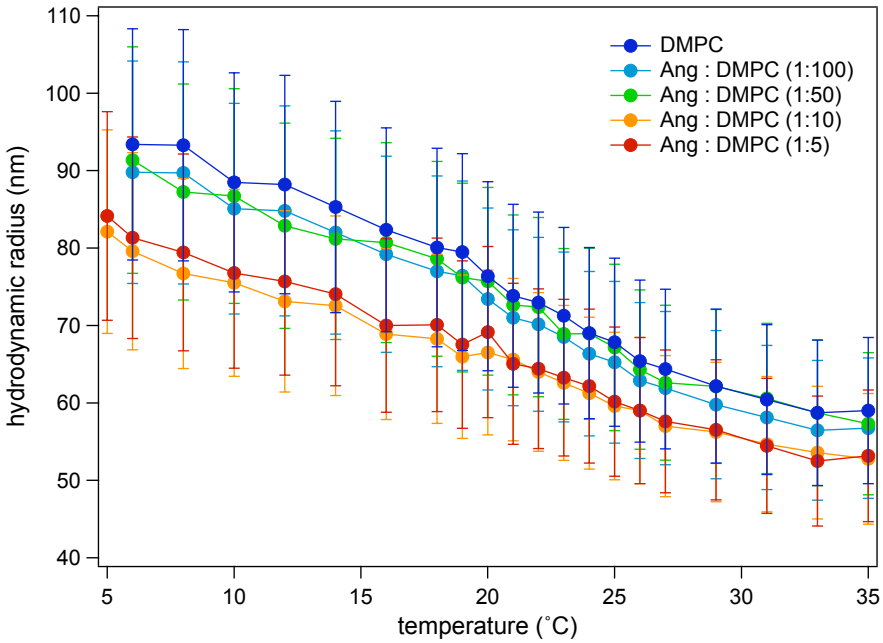

Fig. 2 Dynamic light scattering data showing the hydrodynamic radii calculated for temperatures between 5 and 35 ^{c}irc C. The bars indicate the error, resulting from the polydispersity of the vesicles. The line between the data points is added to provide better visibility

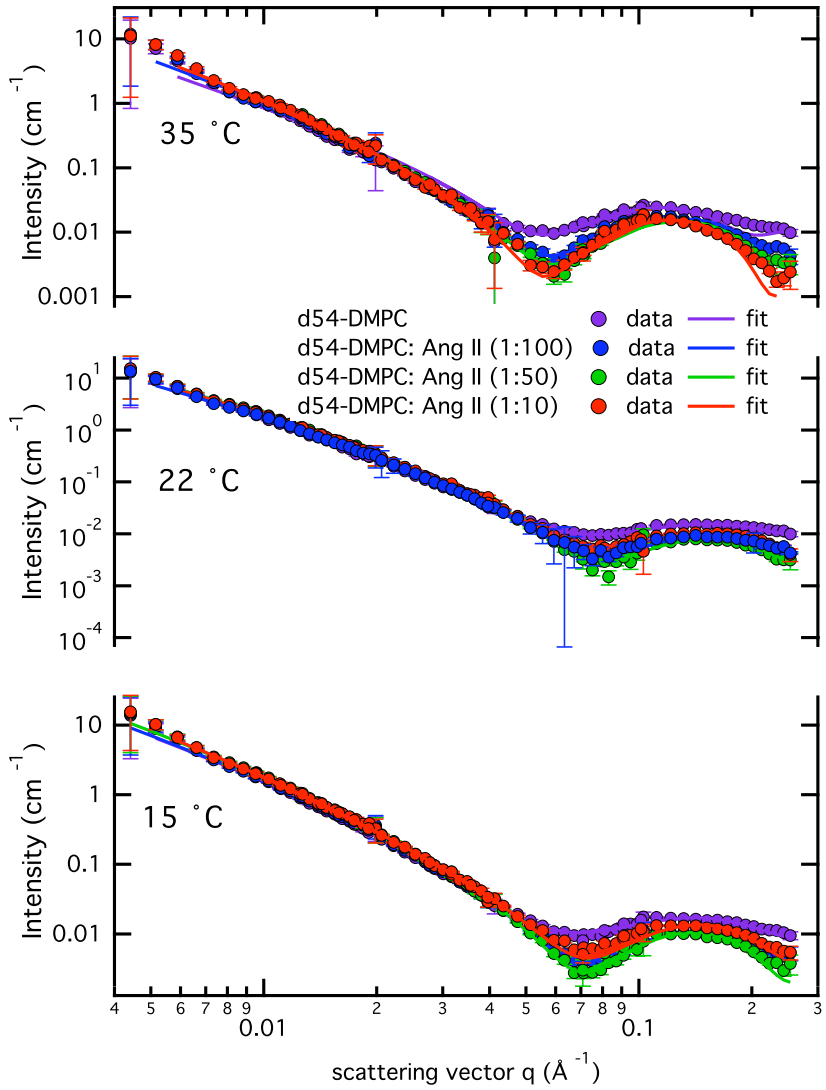

Fig. 3 Small angle scattering data and according fits. Data is shown for experiments on pure d54-DMPC and mixtures of peptide and lipid of 1:100, 1:50, 1:10 and 1:5. The lines indicate the fits performed for the individual data sets.

Acknowledgements This research project has been supported by the European Commission under the 6th Framework Programme through the Key Action: Strengthening the European Research Area, Research Infrastructures. Contract n: RII3-CT-2003-505925. J.P. has been supported by the European Commission under the 6th Framework Programme through the Marie-Curie Action: BIOCONTROL, contract number MCRTN 33439. The authors like to thank the staff of the cSAXS group at the Paul Scherrer Institute for use of the light scattering equipment.

References

ID Alves, N Goasdoué, I Correia, S Aubry, C Galanth, S Sagan, S Lavielle, and G Chassaing. Membrane interaction and perturbation mechanisms induced by two cationic cell penetrating peptides with distinct charge distribution. *BBA-General Subjects*, 1780(7-8): 948–959, 2008.

P Balgavý, M Dubnicková, N Kucerka, M A Kiselev, S P Yaradaikin, and D Uhríková. Bilayer thickness and lipid interface area in unilamellar extruded 1,2-diacylphosphatidylcholine liposomes: a small-angle neutron scattering study. *Biochim Biophys Acta*, 1512(1):40–52, May 2001.

P Bartlett and R Ottewill. A neutron-scattering study of the structural of a bimodal colloidal crystal. *J Chem Phys*, 96(4):3306–3318, Jan 1992.

G Bruylants, J Wouters, and C Michaux. Differential scanning calorimetry in life science: thermodynamics, stability, molecular recognition and application in drug design. *Current Medicinal Chemistry*, 12(17):2011–20, Jan 2005.

D Chansel, T Bizet, S Vandermeersch, P Pham, B Levy, and R Ardaillou. Differential regulation of angiotensin ii and losartan binding sites in glomeruli and mesangial cells. *Am J Physiol*, 266(3 Pt 2):F384–93, Mar 1994.

NJ Cho and SA Asher. Uv resonance raman and absorption studies of angiotensin ii conformation in lipid environments. *Biospectroscopy*, 2(2):71–82, Jan 1996.

O Costerousse, E Jaspard, L Wei, P Corvol, and F Alhenc-Gelas. The angiotensin i-converting enzyme (kininase ii): molecular organization and regulation of its expression in humans. *Journal of Cardiovascular Pharmacology*, 20 Suppl 9:S10–5, Jan 1992.

M de Gasparo, K J Catt, T Inagami, J W Wright, and T Unger. International union of pharmacology. xxiii. the angiotensin ii receptors. *Pharmacol Rev*, 52(3):415–72, Sep 2000.

L Dézsi. Fibrinolytic actions of ace inhibitors: a significant plus beyond antihypertensive therapeutic effects. *Cardiovascular Research*, 47(4):642–4, Sep 2000.

JE Dimsdale, O Kolterman, J Koda, and R Nelesen. Effect of race and hypertension on plasma amylin concentrations. *Hypertension*, 27(6):1273–1276, Jan 1996.

V Fatigati and M J Peach. Development of a new fluorescent angiotensin ii probe. *Am J Physiol*, 255(4 Pt 1):C452–8, Oct 1988.

G W Feigenson. Phase boundaries and biological membranes. *Annual review of biophysics and biomolecular structure*, 36:63–77, Jan 2007.

J Gallová, D Uhríková, N Kucerka, J Teixeira, and P Balgavý. Hydrophobic thickness, lipid surface area and polar region hydration in monounsaturated diacylphosphatidylcholine bilayers: Sans study of effects of cholesterol and beta-sitosterol in unilamellar vesicles. *Biochim Biophys Acta*, 1778(11):2627–32, Nov 2008.

K C Garcia, P M Ronco, P J Verroust, A T Brünger, and L M Amzel. Three-dimensional structure of an angiotensin ii-fab complex at 3 a: hormone recognition by an anti-idiotypic antibody. *Science*, 257(5069):502–7, Jul 1992.

Mikyung Han, Yuan Mei, Htet Khant, and Steven J Ludtke. Characterization of antibiotic peptide pores using cryo-em and comparison to neutron scattering. *Biophysical Journal*, 97(1):164–172, Jan 2009.

T Heimburg. A model for the lipid pretransition: Coupling of ripple formation with the chain-melting transition. *Biophysical Journal*, 78(3):1154–1165, Jan 2000.

Fang Hong, Luo Ming, Sheng Yi, Li Zhanxia, Wu Yongquan, and Liu Chi. The antihypertensive effect of peptides: A novel alternative to drugs?, Jan 2008.

H W Huang. Action of antimicrobial peptides: two-state model. *Biochemistry*, 39(29): 8347–52, Jul 2000.

Ken Jacobson, Ole Mouritsen, and Richard Anderson. Lipid rafts: at a crossroad between cell biology and physics. *Nat Cell Biol*, 9(1):7–14, 2007. 10.1038/ncb0107-7.

I Javierre, F NALLET, AM Bellocq, and M Maugey. Structure and dynamic properties of a polymer-induced sponge phase. *J. Phys.: Condens. Matter*, 12:A295–A299, 2000.

M P Joseph, B Maigret, J C Bonnafous, J Marie, and H A Scheraga. A computer modeling postulated mechanism for angiotensin ii receptor activation. *J Protein Chem*, 14(5):381–98, Jul 1995.

David Jung, Jon Paul Powers, Suzana K Straus, and Robert E W Hancock. Lipid-specific binding of the calcium-dependent antibiotic daptomycin leads to changes in lipid polymorphism of model membranes. *Chemistry and Physics of Lipids*, 154(2):120–8, Aug 2008.

M Kiselev, P Lesieur, AM Kisselev, D Lombardo, and V Aksenov. Model of separated form factors for unilamellar vesicles. *Applied Physics A: Materials Science & Processing*, Jan 2002.

M A Kiselev, E V Zemlyanaya, V K Aswal, and R H H Neubert. What can we learn about the lipid vesicle structure from the small-angle neutron scattering experiment? *Eur Biophys J*, 35(6):477–93, Aug 2006.

SR Kline. Reduction and analysis of sans and usans data using igor pro. *J Appl Crystallogr*, 39(6):895–900, 2006.

W Knoll, J Haas, HB Stuhrmann, HH Fuldner, H Vogel, and E Sackmann. Small-angle neutron scattering of aqueous dispersions of lipids and lipid mixtures. a contrast variation study. *J Appl Crystallogr*, 14(3):191–202, 1981a.

W Knoll, K Ibel, and E Sackmann. Small-angle neutron scattering study of lipid phase diagrams by the contrast variation method. *Biochemistry*, 20(22):6379–83, Oct 1981b.

C Koukoulitsa, I Kyrikou, C Demetzos, and T Mavromoustakos. The role of the anticancer drug vinorelbine in lipid bilayers using differential scanning calorimetry and molecular modeling. *Chemistry and Physics of Lipids*, 144(1):85–95, 2006.

N Kucerka, J F Nagle, J N Sachs, S E Feller, J Pencer, A Jackson, and J Katsaras. Lipid bilayer structure determined by the simultaneous analysis of neutron and x-ray scattering data. *Biophysical Journal*, 95(5):2356–67, Sep 2008.

N Kucerka, M Nieh, and J Katsaras. Asymmetric distribution of cholesterol in unilamellar vesicles of monounsaturated phospholipids. *Langmuir : the ACS journal of surfaces and colloids*, 25(23):13522–7, Dec 2009.

N Kučerka, M Nieh, J Pencer, and T Harroun. The study of liposomes, lamellae and membranes using neutrons and x-rays. *Current Opinion in Colloid & Interface Science*, Jan 2007.

N Kucerka, J Pencer, J N Sachs, J F Nagle, and J Katsaras. Curvature effect on the structure of phospholipid bilayers. *Langmuir*, 23(3):1292–1299, Jan 2007.

Mazen Kurdi, Walmor C De Mello, and George W Booz. Working outside the system: an update on the unconventional behavior of the renin-angiotensin system components. *Int J Biochem Cell Biol*, 37(7):1357–67, Jul 2005.

C Labinjoh, D E Newby, P Dawson, N R Johnston, C A Ludlam, N A Boon, and D J Webb. Fibrinolytic actions of intra-arterial angiotensin ii and bradykinin in vivo in man. *Cardiovascular Research*, 47(4):707–14, Sep 2000.

BM Lowe and DG Smith. Glass electrode measurements in deuterium oxide. *Analytical Letters*, 6(10):903–907, 1973.

S J Ludtke, K He, W T Heller, T A Harroun, L Yang, and H W Huang. Membrane pores induced by magainin. *Biochemistry*, 35(43):13723–8, Oct 1996.

Anna Lundquist, Per Wessman, Adrian R Rennie, and Katarina Edwards. Melittin-lipid interaction: a comparative study using liposomes, micelles and bilayer disks. *Biochim Biophys Acta*, 1778(10):2210–6, Oct 2008.

S MacMahon, R Peto, J Cutler, R Collins, P Sorlie, J Neaton, R Abbott, J Godwin, A Dyer, and J Stamler. Blood pressure, stroke, and coronary heart disease. part 1, prolonged differences in blood pressure: prospective observational studies corrected for the regression dilution bias. *Lancet*, 335(8692):765–74, Mar 1990.

P Mariani, R Casadio, F Carsughi, M Ceretti, and F Rustichelli. Structural analysis of membranes from photosynthetic bacteria by sans. *Europhys Lett*, 37(6):433–438, Jan 1997.

PC Mason, BD Gaulin, RM Epand, GD Wignall, and JS Lin. Small angle neutron scattering and calorimetric studies of large unilamellar vesicles of the phospholipid dipalmitoylphosphatidylcholine. *Phys. Rev. E*, 59(3):3361–3367, Jan 1999.

T Mavromoustakos, E Theodoropoulou, C Dimitriou, JM Matsoukas, D Panagiotopoulos, and A Makriyannis. Interactions of angiotensin ii with membranes using a combination of differential scanning calorimetry and 31p nmr spectroscopy. *Lett Pept Sci*, 3(4):175–180, 1996.

J F Nagle and S Tristram-Nagle. Structure of lipid bilayers. *Biochim Biophys Acta*, 1469 (3):159–95, Nov 2000.

F Nallet, R Laversanne, and D Roux. Modeling x-ray or neutron-scattering spectra of lyotropic lamellar phases - interplay between form and structure factors. *J Phys II*, 3(4): 487–502, Jan 1993.

JM Neutel, DHG Smith, and MA Weber. Is high blood pressure a late manifestation of the hypertension syndrome? *American Journal of Hypertension*, 12(12):215S–223S, Jan 1999.

U.S. Department of health and human services. The seventh report of the joint national commitee on prevention, detection, evaluation, and treatment of high blood pressure. pages 1–52, Dec 2003.

World Health Organization. Diet, nutrition and the prevention of chronic diseases. page 160, Apr 2003.

G Pabst, S Grage, S Dannerpongratz, W Jing, A Ulrich, A Watts, K Lohner, and A Hickel. Membrane thickening by the antimicrobial peptide pgla. *Biophysical Journal*, 95(12): 5779–5788, Dec 2008.

A S Pachori, M J Huentelman, S C Francis, C H Gelband, M J Katovich, and M K Raizada. The future of hypertension therapy: sense, antisense, or nonsense? *Hypertension*, 37(2 Part 2):357–64, Feb 2001.

J Pencer and F R Hallett. Small-angle neutron scattering from large unilamellar vesicles: an improved method for membrane thickness determination. *Physical review E, Statistical physics, plasmas, fluids, and related interdisciplinary topics*, 61(3):3003–8, Mar 2000.

J Pencer, T Mills, V Anghel, S Krueger, R M Epand, and J Katsaras. Detection of submicron-sized raft-like domains in membranes by small-angle neutron scattering. *The European physical journal E, Soft matter*, 18(4):447–58, Dec 2005a.

J Pencer, M Nieh, T A Harroun, S Krueger, C Adams, and J Katsaras. Bilayer thickness and thermal response of dimyristoylphosphatidylcholine unilamellar vesicles containing cholesterol, ergosterol and lanosterol: a small-angle neutron scattering study. *Biochim Biophys Acta*, 1720(1-2):84–91, Dec 2005b.

M V Petoukhov and D I Svergun. Joint use of small-angle x-ray and neutron scattering to study biological macromolecules in solution. *Eur Biophys J*, 35(7):567–76, Sep 2006.

M Ruiz-Ortega, M Ruperez, V Esteban, and J Egido. Molecular mechanisms of angiotensin ii-induced vascular injury. *Current Hypertension Reports*, 5(1):73–9, Feb 2003.

H Schmiedel, L Almasy, and G Klose. Multilamellarity, structure and hydration of extruded popc vesicles by sans. *Eur Biophys J Biophy*, 35(3):181–189, Jan 2006.

GWJ Seto, S Marwaha, DM Kobewka, RNAH Lewis, F Separovic, and RN McElhaney. Interactions of the australian tree frog antimicrobial peptides aurein 1.2, citropin 1.1 and maculatin 1.1 with lipid model membranes: differential scanning calorimetric and fourier transform infrared spectroscopic studies. *Bba-Biomembranes*, 1768(11):2787–2800, 2007.

F Severcan, I Sahin, and N Kazanc. Melatonin strongly interacts with zwitterionic model membranes—evidence from fourier transform infrared spectroscopy and differential scanning calorimetry. *Bba-Biomembranes*, 1668(2):215–222, 2005.

YA Shin and S Yoo. Conformational study of angiotensin ii. *Biopolymers*, 38(2), 1996.

Gary E Striker, Francoice Praddaude, Oscar Alcazar, Scott W Cousins, and Maria E Marin-Castano. Regulation of angiotensin ii receptors and extracellular matrix turnover in human retinal pigment epithelium: role of angiotensin ii. *Am J Physiol-Cell Ph*, 295(6):C1633–C1646, Jan 2008.

HB Stuhrmann, N Burkhardt, G Dietrich, R Jünemann, W Meerwinck, M Schmitt, J Wadzack, R Willumeit, J Zhao, and KH Nierhaus. Proton-and deuteron spin targets in biological structure research. *Nuclear Instruments and Methods in Physics Research A*, 356:124–132, 1995.

WK Surewicz and HH Mantsch. Conformational properties of angiotensin-ii in aqueous-solution and in a lipid environment - a fourier-transform infrared spectroscopic investigation. *J Am Chem Soc*, 110(13):4412–4414, Jan 1988.

DI Svergun and MHJ Koch. Small-angle scattering studies of biological macromolecules in solution. *Reports on Progress in Physics*, 66(10):1735–1782, 2003.

W R Taylor. Hypertensive vascular disease and inflammation: mechanical and humoral mechanisms. *Current Hypertension Reports*, 1(1):96–101, Jan 1999.

E Theodoropoulou and D Marsh. Interactions of angiotensin ii non-peptide at1 antagonist losartan with phospholipid membranes studied by combined use of differential scanning calorimetry and electron spin resonance spectroscopy. *Bba-Biomembranes*, 1461(1):135–146, 1999.

E Theodoropoulou and D Marsh. Effect of angiotensin ii non-peptide at(1) antagonist losartan on phosphatidylethanolamine membranes. *Biochim Biophys Acta*, 1509(1-2):346–60, Dec 2000.

S Tung, H Lee, and S R Raghavan. A facile route for creating ”reverse” vesicles: insights into ”reverse” self-assembly in organic liquids. *J Am Chem Soc*, 130(27):8813–7, Jul 2008.

C Leborgne S Lecomte N Leygue D Scherman A Kichler V Burckbuchler, V Wintgens and C Amiel. Development and characterization of new cyclodextrin polymer-based dna delivery systems. *Bioconjug Chem*, 19(12):2311–20, Dec 2008.

G Valensin, M Delfini, and E Gaggelli. Selective 1h-nmr relaxation investigations of membrane-bound drugs in vitro. 2. angiotensin ii. *Biophys Chem*, 24(1):25–31, Jun 1986.

Y Wang, D Qiu, T Cosgrove, and ML Denbow. A small-angle neutron scattering and rheology study of the composite of chitosan and gelatin. *Colloids and Surfaces B: Biointerfaces*, 70(2):254–258, 2009.

P Westh. Experimental approaches to membrane thermodynamics. *Soft Matter*, 5(17):3249–3257, 2009.

R Winter. Synchrotron x-ray and neutron small-angle scattering of lyotropic lipid mesophases, model biomembranes and proteins in solution at high pressure. *Biochimica et Biophysica Acta (BBA)/Protein Structure and Molecular Enzymology*, 1595(1-2): 160–184, 2002.

P Zoumpoulakis, I Daliani, M Zervou, I Kyrikou, E Siapi, G Lamprinidis, E Mikros, and T Mavromoustakos. Losartan's molecular basis of interaction with membranes and at1 receptor. *Chemistry and Physics of Lipids*, 125(1):13–25, Sep 2003.